# ESR identification of radiation-induced oxygen vacancy centers in paratellurite

A. Watterich,* R. H. Bartram, O. R. Gilliam, L. A. Kappers, and G. J. Edwards
*Department of Physics and Institute of Materials Science, University of Connecticut, Storrs, Connecticut 06268*

I. Földvári and R. Voszka
*Research Laboratory for Crystal Physics, Hungarian Academy of Sciences, H-1112 Budapest, Budaörsi út 45, Hungary*
(Received 30 January 1985)

The ESR spectrum of paratellurite ($\alpha$-$TeO_2$) exposed to 1-MeV electron irradiation reveals a single spin-$\frac{1}{2}$ defect in eight inequivalent sites with an anisotropic $g$ value close to the free-electron value. Principal $g$ values are $2.0105\pm0.0005$, $1.9705\pm0.0005$, and $1.9358\pm0.0005$. Resolved hyperfine structure is attributed to magnetic isotopes of tellurium in seven different sites neighboring each defect site. The $g$-value anisotropy together with the hyperfine structure suggest a positively charged, oxygen-vacancy model ($V_O^{\bullet}$) with properties intermediate between those of the $E_1'$ center in $SiO_2$ and the $F^+$ center in alkaline-earth oxides.

## I. INTRODUCTION

Paratellurite ($\alpha$-$TeO_2$) is a transparent material with excellent acousto-optical properties. It is distinguished by high refractive indices and an unusually soft acoustic shear mode of vibration associated with a room-temperature phase transition at 9 kbar.[1] The resultant enhanced piezo-optic constant[2,3] has led to extended practical applications of paratellurite in deflectors, modulators, and tunable optical filters. The tetragonal crystal structure in the low-pressure phase may be regarded as a covalent distortion of the rutile structure.[4]

We are not aware of any previous radiation-damage investigations in this material. By contrast, extensive radiation damage studies have been reported in materials of rutile structure, e.g., $TiO_2$, $SnO_2$, and $GeO_2$.[5,6] It is of interest to compare the defect structure of $TeO_2$ with these more ionic crystals as well as with the more covalent $SiO_2$.

In the present investigation single crystals of paratellurite were subjected to 1-MeV electron irradiation, and the resulting defects were characterized by electron spin resonance (ESR) spectroscopy. Several additional defects are observed in lower concentration, and many related, unstable defects are produced by low-temperature irradiation; these will be described in subsequent publications. The present paper is concerned only with the dominant stable defect produced by prolonged irradiation at room temperature.

Experimental techniques are described in Sec. II, and the results are presented in Sec. III. A model for the defect is proposed in Sec. IV, and the implications are discussed in Sec. V.

## II. EXPERIMENTAL TECHNIQUES

Starting material in the form of $TeO_2$ powder with less than 5 ppm impurities was prepared from Te metal. Single crystals of paratellurite were grown by a balance-controlled Czochralski technique[7] using a platinum crucible and resistance heating. A pulling rate of 1.2 mm/h along the [110] direction and seed rotation of 30 rpm were employed. X-ray oriented samples were cut by a diamond saw, and the typical sample size was $10\times3.5\times3$ mm. The crystal quality was established by acoustic attenuation, spectral transparency, and dislocation density measurements.[8]

Oriented single crystals of paratellurite were subjected to electron irradiation from a Van de Graaff accelerator, operated at 1 MeV with sample nominal current densities of 1—5 $\mu A\,cm^{-2}$ for times up to 10 h. Irradiations were performed both at room temperature (RT) and at liquid-nitrogen temperature (LNT). For the LNT irradiations the sample was immersed in liquid nitrogen. However, for the RT irradiations the sample temperature was not measured or controlled; some sample heating therefore occurred.

All ESR measurements were performed using Varian $E$-3 and $E$-9 X-band spectrometers with the Varian variable temperature accessory and the rectangular $TE_{102}$ cavity. Typical measurements were made at 92 K with a microwave power of 10 mW and a frequency of approximately 9.1 GHz.

## III. EXPERIMENTAL RESULTS

The undoped $TeO_2$ crystal prior to irradiation showed no ESR signal, but electron irradiation at RT produced a single spin-$\frac{1}{2}$ defect with an anisotropic $g$ value slightly less than the free-electron value. The corresponding ESR spectrum is shown in Fig. 1 for $\mathbf{H}||\mathbf{c}$. Pairs of the eight inequivalent Zeeman lines become equivalent in those planes in which we rotated the samples, and collapse to a single line for $\mathbf{H}||\mathbf{c}$. The principal values of the $\tilde{g}$ tensor listed in Table I were determined from the angular variation of the Zeeman lines shown in Fig. 2.

Figure 3 shows the central portion of the spectrum shown in Fig. 1 for $\mathbf{H}||\mathbf{c}$ on an expanded scale. Around the single main line fives pairs of considerably smaller

 

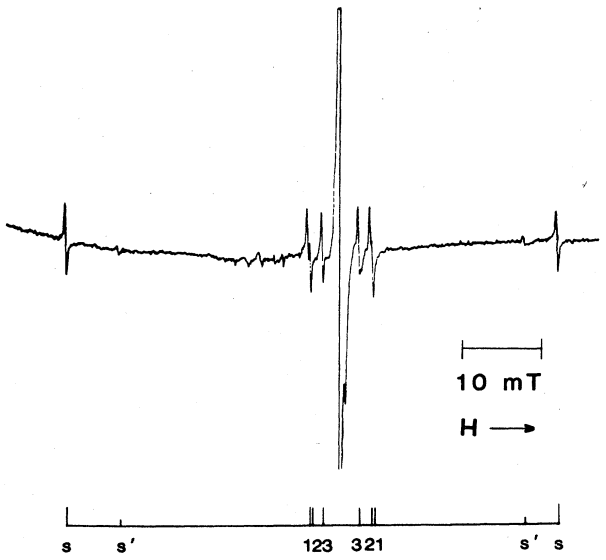


FIG. 1. ESR spectrum for the most prominent defect generated in $TeO_2$ by 1-MeV electron irradiation. This observation was made at approximately 9.1 GHz and 92 K; for this orientation, **H**||**c**, the spectra of eight inequivalent sites are superposed. The central line is at 332.6 mT.

lines are observable. The fact that the lines are paired approximately symmetrically around the main line suggests that they are due to hyperfine interactions with nuclear spins $I=\frac{1}{2}$. The five different hyperfine splittings correspond to different positions of tellurium nuclei around the defect. A sixth pair of hyperfine lines, with highly anisotropic splitting, is distinguishable from the central line in some orientations. The $^{125}$Te isotope has $I=\frac{1}{2}$ and a natural abundance of 6.99%. Most of the Te isotopes are of nuclear spin $I=0$ with natural abundance of 92.14%. From their natural abundances the expected intensity ratio of the single main line and each of the smaller lines is

TABLE I. Principal values and eigenvectors of spin-Hamiltonian tensors for one of the eight inequivalent sites. The estimated errors are ±0.0005 for $g$ values and ±0.003 for eigenvectors of $\overleftrightarrow{g}$; $\pm 3\times 10^{-4}$ cm$^{-1}$ for $A$ values and ±0.03 for eigenvectors of $\overleftrightarrow{A}$. The dimensionless eigenvectors are defined with respect to the edges of the conventional tetragonal unit cell, as shown in Fig. 7.

| | | | |
|---|---|---|---|
| $\overleftrightarrow{g}$ | 2.0105 | 1.9705 | 1.9358 |
| | 0.679 | −0.728 | 0.096 |
| | 0.628 | 0.508 | −0.590 |
| | 0.381 | 0.461 | 0.802 |
| $\overleftrightarrow{A}_s$ ($10^{-4}$ cm$^{-1}$) | 776 | 595 | 533 |
| | 0.750 | 0.012 | 0.661 |
| | −0.614 | 0.383 | 0.690 |
| | −0.245 | −0.924 | 0.295 |
| $\overleftrightarrow{A}_1$ ($10^{-4}$ cm$^{-1}$) | 96 | 78 | 73 |
| | 0.514 | −0.203 | −0.834 |
| | 0.801 | 0.463 | 0.380 |
| | 0.309 | −0.863 | 0.400 |

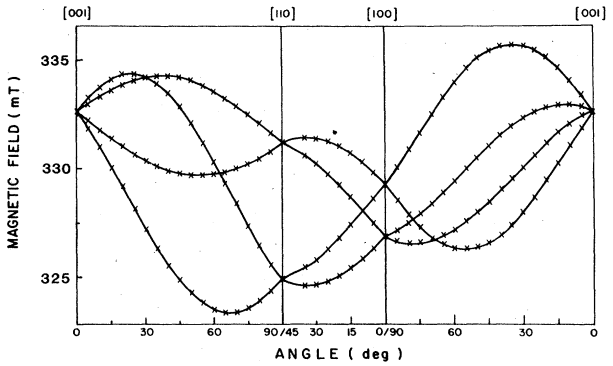


FIG. 2. Angular variation of the Zeeman lines produced in $TeO_2$ by 1-MeV electron irradiation. Only four inequivalent sites are distinguishable in each plane shown here. Observations were made at approximately 9.1 GHz and 92 K.

26, in good agreement with the observed ratio of 29.

With increased gain, it was possible to display the hyperfine lines associated with $^{123}$Te isotopes ($I=\frac{1}{2}$, natural abundance 0.87%) in addition to those with $^{125}$Te isotopes, as shown in Fig. 4. The intensity ratio of hyperfine lines is 7.6, in good agreement with the ratio of isotopic abundances of $^{125}$Te and $^{123}$Te, and the observed ratio of hyperfine splittings is 1.2 in agreement with the ratio of magnetic moments of these isotopes.

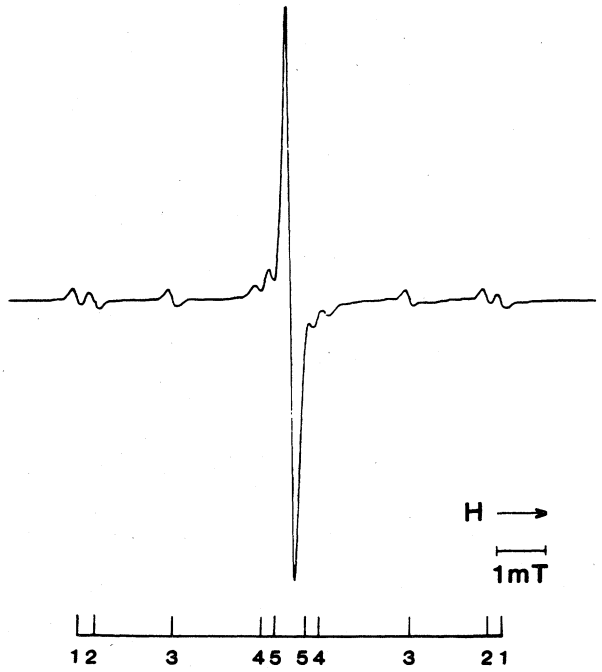


FIG. 3. An expanded ESR sweep of the central portion of Fig. 1 depicting hyperfine interaction of the radiation-induced defect with $^{125}$Te magnetic isotopes (6.99% abundant, $I=\frac{1}{2}$) in five neighboring sites. A smaller splitting due to a sixth site is not resolved from the central line in this orientation. This ESR observation was made at approximately 9.1 GHz and 92 K for **H**||**c**; the central line is at 332.6 mT.

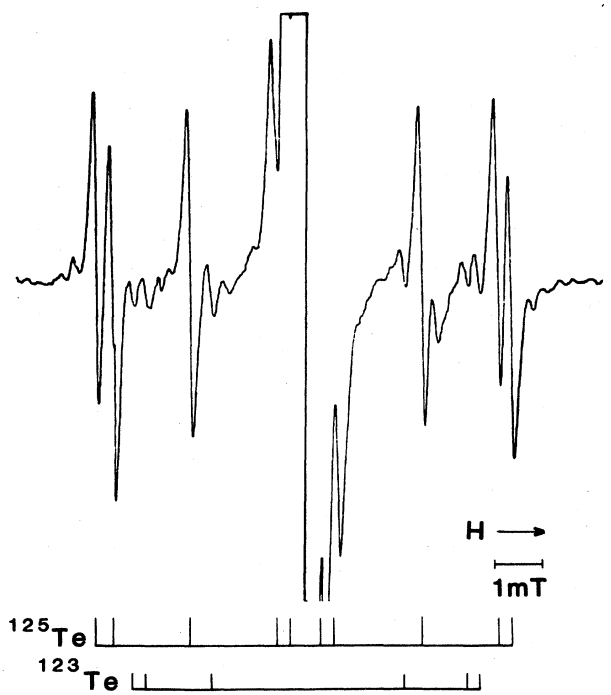


FIG. 4. The same spectrum as in Fig. 3 with amplifier gain increased by a factor of 20. Hyperfine structure associated with $^{123}$Te magnetic isotropes (0.87% abundant, $I=\frac{1}{2}$) in three neighboring sites can be distinguished.

Additional lines, labeled $s$, and $s'$, are observed on both the low- and high-field sides of the strong central line in Fig. 1. The low-field spectrum is shown in detail in Fig. 5 at a higher gain setting. It comprises a single principal line (labeled $s$) with a single smaller satellite (labeled $s'$) on its high-field side, and still smaller pairs of satellites symmetrically disposed about the principal line in a pattern identical to that of the hyperfine structure associated with the central ESR line near $g=2$. The high-field spectrum is essentially similar to the low-field spectrum, except that the single smaller ($s'$) satellite occurs on the low-field side of the principal line ($s$). Under a variety of growth and annealing conditions, the principal line ($s$) in each case maintains a fixed intensity ratio with the central ESR line, which is the same as that of the $^{125}$Te hyperfine lines shown in Fig. 3. The intensities of the single satellites ($s'$) are lower by a factor of $\approx 8$; i.e., the same as the $^{123}$Te hyperfine lines shown in Fig. 4. Finally, the intensities of the satellite pairs are less than those of the principal lines by a factor of $\approx 26$, and therefore less than that of the central line by a factor of approximately $(26)^2=676$.

The conclusion is inescapable that the additional low- and high-field spectra represented by ($s$) and ($s'$) are in fact additional hyperfine lines corresponding to a much stronger tellurium hyperfine interaction than those of Figs. 3 and 4. The observed ESR spectra correspond to those centers which have either no magnetic isotopes among their proximate tellurium neighbors (the central line), only one magnetic isotope (the hyperfine structure of Figs. 1, 3, and 4) or two magnetic isotopes (the satellite

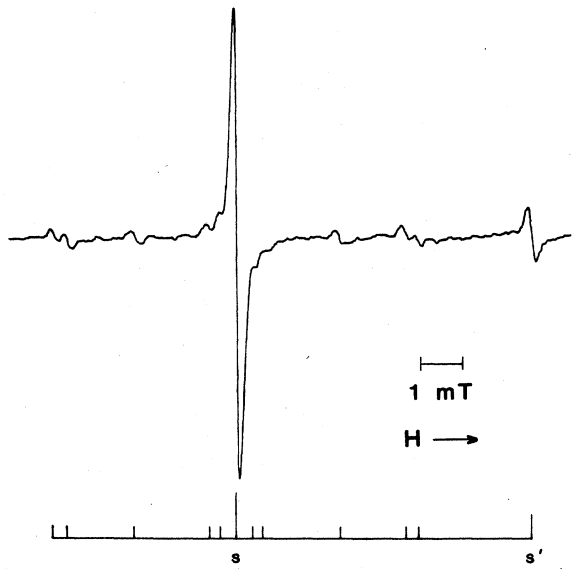


FIG. 5. An expanded portion of the ESR spectrum shown in Fig. 1, centered on the low-field line labeled $s$. Observations were made at approximately 9.1 GHz and 92 K for $\mathbf{H}||\mathbf{c}$; the magnetic field at $s$ was 294.9 mT.

pairs of Fig. 5). These spectra are described by a spin Hamiltonian of the form

$$\mathcal{H}_S=\mu_B\mathbf{H}\cdot\overleftrightarrow{\mathbf{g}}\cdot\mathbf{S}+\sum_i \mathbf{S}\cdot\overleftrightarrow{\mathbf{A}}_i\cdot\mathbf{I}_i\ , \tag{1}$$

with $S=\frac{1}{2}$ and $I_i=\frac{1}{2}$, where the subscript $i$ in the second term denotes one of the two magnetic isotopes in one of the neighboring tellurium sites, and the sum extends over the number of magnetic isotopes present (0, 1, or 2). The asymmetrical disposition of the strongly split hyperfine lines $s$ and $s'$, which is evident from Fig. 1, is readily explained as a second-order effect. In an approximation in which the anisotropy of the $\overleftrightarrow{\mathbf{g}}$ and $\overleftrightarrow{\mathbf{A}}$ tensors is neglected, the magnetic field required for resonance is given approximately by the expression

$$g\beta H/h\nu=1\pm A/2h\nu-(A/2h\nu)^2\ . \tag{2}$$

Values of the strong hyperfine constants obtained from Eq. (2) by averaging over magnetic-field orientations are $A_s/h\nu=0.213$ and $A_{s'}/h\nu=0.176$ for the $^{125}$Te and $^{123}$Te isotopes, respectively. The ratio $A_s/A_{s'}$ is the same as that of the respective magnetic moments, $\mu(^{125}\text{Te})/\mu(^{123}\text{Te})=1.2$, and the observed asymmetry for each isotope is well described by the third term on the right-hand side of Eq. (2).

The angular variations for resonances due to the strongest hyperfine interaction are shown in Fig. 6 on the low- and high-field sides of the angular variation of the central Zeeman lines. They reflect the combined effects of the anisotropy of the $\overleftrightarrow{\mathbf{g}}$ and $\overleftrightarrow{\mathbf{A}}_s$ tensors. The angular variations of the hyperfine lines marked $s'$ in Figs. 1 and 5 appear to be essentially similar but with a reduced $\overleftrightarrow{\mathbf{A}}$ tensor. Of the resolved hyperfine splittings, only those associated with $^{125}$Te($s$) and $^{125}$Te(1) are sufficiently anisotropic and well resolved to permit determination of both principal

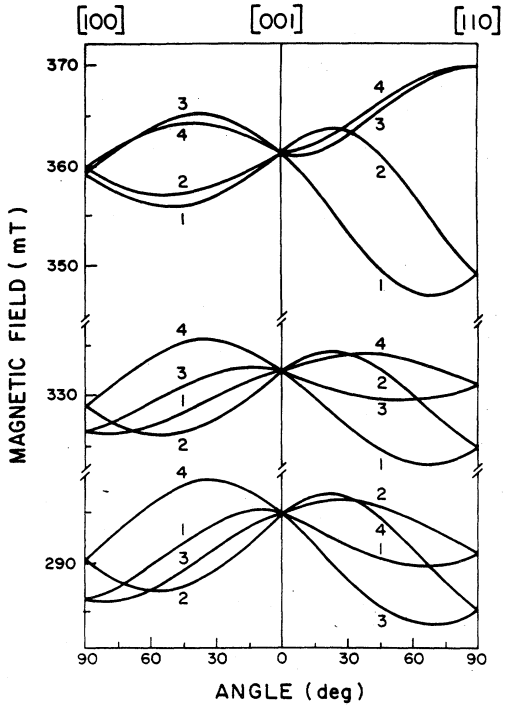


FIG. 6. ESR angular variations of the strongest hyperfine interaction, labeled as *s* in Figs. 1 and 5, plotted on the low- and high-field sides of the angular variations for the central Zeeman lines. All resonances are numbered in accordance with distinguishable inequivalent sites within each plane. (There are actually eight inequivalent sites which are paired differently in the different planes.) The superficial resemblance of the central and low-field spectra is misleading, since lines corresponding to different inequivalent sites do not occur in the same sequence in the two spectra. Observations were made at approximately 9.1 GHz and 92 K.

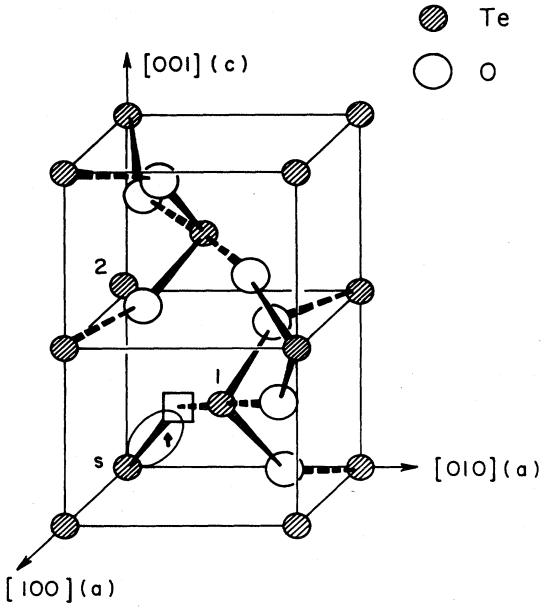


FIG. 7. Model for the most prominent radiation-induced defect in $TeO_2$: a positively charged oxygen vacancy, which is designated as a $V_0^{\bullet}$ center (represented by the square). The three largest $^{125}Te$ hyperfine splittings are tentatively attributed to the three neighboring cations numbered according to the convention of Fig. 1. The unpaired spin is concentrated preferentially on the tellurium atom marked *s*. Short bonds are indicated by heavy solid lines and long bonds by heavy dashed lines.

values and principal axes of the hyperfine tensor. These quantities are listed in Table I. The $^{125}Te(2)$ and $^{125}Te(3)$ hyperfine splittings are more nearly isotropic, and it is not feasible to follow the angular variations of the remaining hyperfine lines.

In pure $TeO_2$ the ESR spectrum associated with this center showed no tendency to saturate, even after a cumulative dose of $1\times10^{18}$ $e/cm^2$ at RT. This center could be detected under a variety of radiation conditions at LNT and at RT. Under thermal treatment the center becomes unstable above 250 °C.

## IV. DISCUSSION

In the paratellurite phase, $TeO_2$ has the tetragonal space group $P4_12_12$ or $D_4^4$. The tetragonal crystal structure of paratellurite may be regarded as a distorted rutile structure, with doubling of the unit cell along the *c* axis. The positions of the telluriums are shifted from the regular rutile positions; however, the size of the shifts is very small. Tellurium is fourfold coordinated by oxygen, the coordination polyhedron being a somewhat distorted trigonal bipyramid with two different bond distances. (See Fig. 7.) Eight inequivalent oxygen sites can be distinguished for an arbitrary magnetic field orientation, four for **H** in (100), (110), and (001) planes, and one for **H**||c. The distortion of paratellurite from the rutile structure is attributable to covalency.[4] As a consequence of this distortion, each oxygen atom in paratellurite is bonded to two tellurium atoms with an angle of 140° between long and short bonds; other tellurium neighbors are at somewhat larger distances.

The ESR spectrum produced by 1-MeV electron irradiation reveals a spin-$\frac{1}{2}$ defect in eight inequivalent sites, with an anisotropic *g* value close to the free-electron value, which does not appear to saturate with radiation dose. These data are compatible with an oxygen-vacancy model for the defect which has a net charge $+e$ with respect to the perfect crystal; i.e., a $V_0^{\bullet}$ center in the Kroger-Vink notation.[9] The ESR spectrum resembles that of the corresponding center in $SiO_2$, the $E_1'$ center,[10,11] but with the *g*-value anisotropy scaled approximately in the ratio of spin-orbit constants, $\lambda(Te^{3+})/\lambda(Si^{+})=32$.[12] Furthermore, the resolved hyperfine structure reveals that the unpaired spin is localized preferentially on one tellurium atom adjacent to the oxygen vacancy in $TeO_2$, just as the unpaired spin of the $E_1'$ center is localized on one silicon atom in $SiO_2$.[11,13] However, in $SiO_2$ the two weak hyperfine interactions are two orders of magnitude weaker than the strong interaction, whereas six additional hyperfine interactions are observed in $TeO_2$ which are only one order of magnitude weaker than the strong interaction.

Evidently, the unpaired spin is less localized in $TeO_2$ than in $SiO_2$. Thus the $V_0^{\bullet}$ center in $TeO_2$ has properties intermediate between those of the $E_1'$ center in $SiO_2$ and the $F^+$ center in alkaline-earth oxides[14] where the unpaired spin occupies a diffuse, vacancy-centered wave function. Our model for the defect is illustrated in Fig. 7.

The $E_1'$ center in $SiO_2$ has nearly axial symmetry about a Si—O bond direction, which is reflected in both the $\overleftrightarrow{g}$ tensor and the $\overleftrightarrow{A}$ tensor for the strong hyperfine interaction.[11,13] This axial symmetry is preserved in the distortion, which effects the localization of unpaired spin on one silicon atom.[15] By contrast, the corresponding $V_0^{\bullet}$ center in $TeO_2$ has no symmetry, and the principal axes of the $\overleftrightarrow{g}$ tensor and the $\overleftrightarrow{A}$ tensors are not strongly correlated.

The ESR spectrum of the $V_0^{\bullet}$ center in $TeO_2$ bears some resemblance to that of the substitutional tellurium double-donor impurity in Si in its singly ionized state, $Te^+$.[16] The latter ESR spectrum is isotropic as a consequence of tetrahedral site symmetry, but it also exhibits an asymmetric hyperfine splitting associated with $^{125}Te$ and $^{123}Te$ magnetic isotopes, and a much weaker transferred hyperfine interaction with Si neighbors. The magnitude of the hyperfine constant for $Si:Te^+$ is twice that of the isotropic part of the hyperfine constant in the present spectrum. This observation is consistent with the inference of substantial delocalization of unpaired spin density in the $V_0^{\bullet}$ center in $TeO_2$.

## V. CONCLUSION

We have established that paratellurite is subject to radiation damage by 1-MeV electron irradiation. The most prevalent radiation-induced defect, the $V_0^{\bullet}$ center, is found to have properties intermediate between the $E_1'$ center in $SiO_2$ and the $F^+$ center in alkaline-earth oxides. Many additional defects have also been observed in irradiated $TeO_2$ which appear to be defect or impurity-related variants of the $V_0^{\bullet}$ center. These perturbed centers will be described elsewhere.

*Note added in proof.* An article published after acceptance of the present manuscript [N. P. Baran, A. A. Bugai, V. G. Grachev, N. I. Deryugima, and L. G. Dovchenko, Fiz. Tverd. Tela (Leningrad) **27**, 564 (1985)] appears to concern the same defect, produced by gamma radiation; however, incomplete ESR spectra are presented and no model is proposed.

## ACKNOWLEDGMENTS

The authors are grateful to Professor Frank Feigl and Professor Beall Fowler for a helpful discussion, and Professor David Madacsi and Mr. Paul Generous for expert technical assistance. This research was partially supported by the U.S. National Science Foundation under Grant No. INT-8219077, by the Hungarian Academy of Sciences, and by the University of Connecticut Research Foundation.

*Permanent address: Research Laboratory for Crystal Physics, Hungarian Academy of Sciences, H-1112 Budapest, Budaörsi út 45, Hungary.

[1]P. S. Peercy and I. J. Fritz, Phys. Rev. Lett. **32**, 466 (1974).
[2]N. Uchida and Y. Ahmachi, J. Appl. Phys. **40**, 4692 (1969).
[3]T. Yano and A. Watanabe, J. Appl. Phys. **45**, 1243 (1974).
[4]O. Lindquist, Acta Chem. Scand. **22**, 977 (1968).
[5]R. A. Weeks, in *Recent Advances in Science and Technology of Materials,* edited by A. Bishay (Plenum, New York, 1974), Vol. I, p. 27.
[6]L. A. Kappers, O. R. Gilliam, and M. Stapelbroek, Phys. Rev. B **17**, 4199 (1978).
[7]F. Schmidt and R. Voszka, Cryst. Res. Technol. **16**, K127 (1981).
[8]I. M. Silvestrova, Yu. V. Pisarevskii, I. Földvári, A. Peter, R. Voszka, and J. Jánszky, Phys. Status Solidi A **66**, K55 (1981).
[9]F. A. Kröger, F. Stieltjes and H. J. Vink, Philips Res. Rep. **14**, 557 (1959).
[10]R. A. Weeks, J. Appl. Phys. **27**, 1376 (1956).
[11]R. H. Silsbee, J. Appl. Phys. **32**, 1459 (1961).
[12]C. E. Moore, in *Atomic Energy Levels,* Natl. Bur. Stand. (U.S.) Spec. Publ. No. 467 (U.S. GPO, Washington, D.C. 1971), Vols. I and III.
[13]M. G. Jani, R. B. Bossoli, and L. E. Halliburton, Phys. Rev. B **27**, 2285 (1983).
[14]B. Henderson and J. E. Wertz, *Defects in Alkaline Earth Oxides* (Taylor and Francis, London, 1977).
[15]K. L. Yip and W. B. Fowler, Phys. Rev. B **11**, 2327 (1975).
[16]H. G. Grimmeiss, E. Janzen, H. Ennen, O. Schirmer, J. Schneider, R. Worner, C. Holm, E. Sirtl, and P. Wagner, Phys. Rev. B **24**, 4571 (1981).